DOI: 10.1002/ ((please add manuscript number))
Article type: Full Paper

Spatial Organization in Proteinaceous Membrane-Stablized Coacervate Protocells

Junbo Li, Xiaoman Liu, Loai K. E. A. Abdelmohsen,David S. Williams* and Xin Huang**

((Optional Dedication))

J. B. Li, Dr. X.M. Liu, Prof. X. Huang
MIIT Key Laboratory of Critical Materials Technology for New Energy Conversion and Storage, School of Chemistry and Chemical Engineering, Harbin Institute of Technology, Harbin 150001, China
E-mail: xinhuang@hit.edu.cn
Dr. L.K. E.A. Abdelmohsen
Department of Chemical Engineering and Chemistry, Eindhoven University of Technology, Eindhoven 5600 MB, The Netherlands
E-mail: l.k.e.a.abdelmohsen@tue.nl
Dr. D. S. Williams
Department of Chemistry, Swansea University, Swansea SA2 8PP, United Kingdom
E-mail: d.s.williams@swansea.ac.ul

Keywords: coacervate, protocell, spatial organization, proteinaceous membrane, proteinosome

As a model protocell, membrane-free coacervate microdroplet has been widely utilized in functional studies to provide insights into the physicochemical properties of the cell and to engineer cytomimetic soft technologies, however, the lack of a discrete membrane contributed to its instability and limited further application. Herein, we developed a strategy to fabricate a hybrid protocell based on the self-assembly of a proteinaceous membrane at the surface of coacervate microdroplet driven by a combination of electrostatic adhesion and steric/hydrophilic surface buoyancy. The semi-permeable proteinaceous membrane could enhance coacervate stability obviously without compromising sequestration behavior. Significantly, such hybrid protocells demonstrated spatial organization whereby various functional enzymes could be located in discrete regions, which facilitated an on/off modulation for a cascade enzymatic reaction along with enhanced chemical communication between sub-populations.

1. Introduction

Cells are the fundamental structural and functional unit of all living organisms. The design and engineering of microcompartments that mimic the unique structure and function of cells has received increasing attention in recent years.[1] Artificial micro-systems (or 'protocells') that exhibit bio-functional properties such as compartmentalization, metabolism, communication and replication, are invaluable tools that researchers can utilize as they seek to understand the origin and evolution of early life.[2] Examples of such protocells include membrane-bound structures such as lipid vesicles,[3] polymersomes,[4] colloidosomes[5] or proteinosomes,[6] and membrane-free structures such as coacervate microdroplets,[7] hydrogels[8] and aqueous two-phase systems (ATPS).[2a,9] These physical platforms have been integrated with functional components and exploited in the study of, for example, cell-free gene transcription and translation,[10] chemical signal communication and transfer,[11] enzyme-mediated cascade,[12] growth, reproduction and division.[13] Protocellular platforms are typically engineered in a bottom-up fashion, constructed using various molecular components (and process) in the laboratory.[14] While first generation protocells have sought to mimic basic behaviors of cellular life, the scope of possible research is limited by their rudimentary chemical form. By developing more sophisticated molecular pathways for the engineering of protocells (via spontaneous self-assembly), next generation platforms can be developed that more closely mimic the hierarchical complexity of the cell in order to gain chemical insights into the emergence (and development) of cellular compartments.[15] For example, the self-assembly of fatty-acid and lipid vesicles (as a prototype in the origin of life) have been utilized to construct protocell, the resulting structure are static and incapable of dynamically interacting with their environment to enhance their complexity. Therefore, although the biological ubiquity of lipids is

irrefutable, it remains necessary to explore pathways of compartmentalization in order to understand the molecular origins of prebiotic cellularity.

Complex coacervation is a liquid-liquid phase separation (LLPS) phenomenon that occurs through electrostatic complexation of oppositely charged polyelectrolytes and subsequent de-mixing into a condensed (polymer-rich) phase, with unique properties such as reduced polarity, increased viscosity and ability to sequester macromolecular species.[7] Biologically, coacervate formation is associated with intracellular phase separation processes through formation of Cajal bodies,[16] P granules[17] and stress granules[18] during, for example, mitosis.[19] Under certain conditions (such as polymer concentration and mixing stoichiometry) coacervates form metastable microdroplets that have been presented as a protocell model uniquely exhibiting dynamic compartmentalization, capable of spontaneously concentrating biological molecules and enhancing their activity.[20] Coacervates exhibit dynamic partitioning and uptake of molecular due to their reduced dielectric constant, as compared to the surrounding water phase, enabling spatial compartmentalization and chemical enrichment without lipidic molecules.[20a,21] Although membrane-free coacervates demonstrate many advantageous properties, the absence of an enclosing membrane critically limits their stability and negates their ability to discretize chemical information, which severely hampers their application towards micro-compartmentalization as compared to membranous protocell whereby the protective properties of chemical membranes can be combined with the crowded (cytosolic) interior of coacervates, via spontaneous interfacial assembly and membranization. Polyoxometalate clusters,[22] colloidal silica particles,[23] fatty acid[24] and lipids[25] have shown some ability to assemble on the coacervate surface, forming a protective membrane with limited chemical versatility. In order to address this critical protocellular milestone, amphiphilic terpolymer molecules were synthetized that were

capable of spontaneously forming a discrete membrane at the coacervate interface. This terpolymer membrane effectively stabilized against droplet coalescence and structural deformation; yielding a hierarchical protocell capable of displaying advanced chemical communication.[26]

The formation of protein-based membranous protocells ('proteinosomes') has recently been developed via interfacial assembly of polymer-conjugated enzymes at the interface of a water/isooctanol emulsion.[6] Proteinosomes show effective encapsulation of guest-molecule, gene-directed protein synthesis, size-selective membrane permeability and multicompartmentalization – an example of cytomimetic engineering for biology and biomaterials research.[2c,6,27] The ability of proteins to undergo unique interfacial behaviors when exposed to coacervate droplets was recently demonstrated by the formation of unique structures at the external coacervate surface following interaction with filamentous protein (FtsZ).[28] The capacity of proteins to undergo (directed) interfacial assembly affords unique opportunities to study the properties of a functional membrane and generate microsystems with carefully engineered spatial ordering of functional cascades.[12] Herein, we present a hybrid hierarchical protocell model based on the spontaneous self-assembly of a proteinaceous membrane at the external interface of coacervate microdroplets. Protein-polymer conjugates were engineered in order to spontaneously form such a membrane in aqueous at the external coacervate interface via a combination of electrostatic adhesion and steric/hydrophilic surface buoyancy (**Figure 1**a). We demonstrate the ability of the semi-permeable protein membrane to stabilize coacervate microdroplet against coalescence, creating a discreate inner domain shielded from equilibrium with the surrounding environment. This bottom-up hybrid protocell was capable of spatially integrating functional elements between the membrane and core, where cytomimetic condensation offers opportunities to study chemical communication.

2. Results and Discussion

Polysaccharides are widely used as building blocks in biomaterials engineering because of their biocompatibility, biodegradability and low toxicity.[25a] In this work, we adopted the amylose-based coacervate system previously described, utilizing oppositely charged amylose derivatives that undergo electrostatic binding and phase separation under certain mixing stoichiometries in physiological salt concentrations.[26] Cationic quaternized amylose (Q-Am) was prepared with a degree of substitution (DS) of 0.7 and anionic succinyl amylose (Su-Am) with DS of 1.6-1.75 (DS measured using combination of ^{1}H NMR and, in the case of Su-Am, complexometric titration of Cu^{2+}; Figure S1 and S2, Supporting Information). The appearance of characteristic FTIR absorbances for C=O at 1727 cm^{-1} and $+N(CH_3)_3$ at 1475 cm^{-1} confirmed the successful preparation of these two amylose derivatives (Figure S3, Supporting Information). Coacervation was initiated through electrostatic interaction of oppositely charged polymers in phosphate-buffered saline (PBS). From turbidimetric titration it was clear that coacervation occurred when there was a molar excess of Q-Am over Su-Am, which was due to charge imbalance between the two polyelectrolytes (*ca.* 2.5-fold increase in charge density of Su-Am as compared to Q-Am) requiring greater amounts of Q-Am to neutralize the highly charged Su-Am (Figure S4a, Supporting Information). In terms of salt stability, using a 2:1 stoichiometric ratio, we observed coacervation disassembly when salt concentration exceeded 200 mM (Figure S4b, Supporting Information). For further studies we used a salt concentration of 50 mM. Zeta potential measurements reflected the overall anionic character of our coacervate system, owing to the greater charge of Su-Am over Q-Am, with 2:1 coacervates displaying a value of ca. -23 mV (Figure S4c, Supporting Information). Without

interfacial stabilization, coacervate microdroplets readily coalesced and wetted glass slides (**Figure 2**a).

As a strategy to engineer protein-polymer conjugates that were capable of stabilizing the (negatively charged) coacervate surface we adopted cationization and PEGylation to introduce strong coacervate affinity and steric buoyancy (to prevent sequestration), respectively (Figure 1a). To achieve this, protein (bovine serum albumin, BSA) was first cationized using carbodiimide-mediated coupling with hexamethylene diamine (BSA-NH_2) followed by direct coupling to 5 kDa succinimidyl-terminated monomethoxy-poly (ethylene glycol) (mPEG-BSA) (Figure 1a). Spectroscopic measurements indicated that, after cationization, the number of surface accessible amines increased from *ca.* 21 to 80 (Figure S5 and Table S1, Supporting Information). After mPEG coupling, the average number of polymer chains on BSA-NH_2 was *ca.*12 (Figure S6 and Table S4, Supporting Information). Formation of hybrid protocells was accomplished in solution by mixing a concentrated solution of mPEG-BSA into a suspension of coacervate microdroplets under gentle stirring so that spontaneous membranization occurred (fluorescently-labelled proteins were utilized to enable membrane visualization, Figure 1b). Indeed, the cationic proteins were strongly associated with the anionic coacervate droplets and then the direct sequestration into the condensed phase was successfully prevented by the steric buoyancy of conjugated PEG hydrophilia. The balance between these two factors is the key to achieving spontaneous membranization in this system.

The kinetic of mPEG-BSA assembly around the coacervate microdroplets could be visualized over the course of 1 h; during which time the fluorescence intensity of the membrane increased and levelled off (Figure 1b and 1c). Coacervate microdroplets retained sequestered cargo during this membranization process and the membrane integrity was clearly observable, preventing coalescence (Figure 1d and S7,Supporting

Information). 3D visualization of the hybrid protocell confirmed the spherical (i.e. non-wetted) character of the microdroplet and that the discrete membrane was distinct from excess protein in the surrounding medium (Figure 1e). 3D confocal micrograph also showed that mPEG-BSA could be well around coacervate, resulting in formation of hybrid protocell with integral protein-polymer membrane and the coacervate core (Figure 1e). Electron microscopy showed that the stability of membranized coacervate microdroplets was greatly increased and their spherical morphology was maintained even after drying, coating and during imaging (Figure 1f). During membranization the surface potential of protocells observably decreased from *ca.* -23.5 to -18.3 mV, due to the charge binding of protein-polymer conjugates at the surface (Figure S8, Supporting Information).

Without mPEG-BSA at the interface, coacervate droplets were unstable and coalesced with time, reducing the droplet number rapidly over the course of 30 mins (Figure S9, Supporting Information). In contrast, membranization arrested this coalescence and stabilized the population of droplet-fixing their morphology and size. This demonstrated the significant improvement to the stability of coacervates that was imparted by the protein membrane. To further probe this, we visualized the rapid mixing of uncoated coacervates by tracking the fluorescence signal from separate populations of coacervates (labelled with either fluorescein or rhodamine–Figure 2a). Addition of 50 μL of 50 mg/mL mPEG-BSA to the coacervate suspension (comprising 200 μL of 1 mg/mL Q-Am and 100 μL Su-Am) resulted in enhanced stabilization, although some mixing was evident after 10 mins (Figure 2b). As with terpolymer-mediated membranization of coacervate droplets, incomplete membrane formation yields intermediate stabilization[26]. Addition of increased amounts of protein (100 μL) extends the droplet stability, providing complete surface immobilization without any coalescence (Figure 2c). These observations were attributed to the variable coverage of

mPEG-BSA on the coacervate surface, in a similar fashion to previous work that demonstrated this same phenomenon using a synthetic terpolymer membrane. In this way, the size of hybrid protocells could be controlled by adding protein-polymer conjugates at different time points, arresting coalescence and droplet growth, to generate droplets with sizes of *ca.* 5, 13 and 25 μm with membranization triggered after 0, 2 or 5 mins, respectively (Figure S10, Supporting Information). In this way, membrane-stabilized coacervates have been achieved through interfacial assembly of protein-polymer conjugates – generating a new type of hybrid protocell model.

Having accomplished hybrid protocell fabrication, we explored the functional properties of the system – probing molecular sequestration and the nature of this proteinaceous membrane. Small molecules (such as fluorescein, rhodamine B and nicotinamide adenine dinucleotide) could still permeate the semi-permeable protein-enriched membrane and become sequestered by the inner coacervate lumen (**Figure 3**a-c). In order to probe the porosity of the membrane, FITC-dextran of different molecular weights were employed to observe the cut-off for permeation. Indeed, low molecular weight polymer (MW＜4 kDa) could diffuse into the coacervate lumen whereas above10 kDa this was prevented by the membrane (Figure 3d-f). This is a critical property for protocellular systems, as the cell is made up of various semi-permeable interfaces that regulate molecular transport and communication.

Chemical communication is important for cells so that they can coordinate function and response with neighboring populations. This behavior is mediated by enzyme-catalyzed reactions that initiated by signaling molecules, which are released from and travel between confined environments.[26] In order to mimic this life-like potential of hybrid protocell, we used glucose oxidase (GOx) and horseradish peroxidase (HRP) to initiate enzymatic reactions (**Figure 4**a). To demonstrate the unique capacity of this protocellular platform to engage in enzyme-mediated chemical

communication through the generation of active membranes, whereby functional components can be spatially organized, a number of fluorimetry and colorimetric assays were conducted. In order to showcase the versatile nature of this platform, we sought to mimic chemical signal transfer between internal and interfacial components by generating GOx or HRP membranes where the partner enzyme (HRP/GOx, respectively) was sequestered within the coacervate cytosol. In general, recognition sites on the cellular membrane, which mainly comprise proteins, are used by cells to trigger intracellular responses. Exchanging BSA in the cationized protein conjugates for enzymes (GOx and HRP) successfully resulted in membranized coacervates, imbuing the hybrid protocells with functional aspects. Through spectroscopic measurements (using a colorimetric substrate) it was determined that mPEG-GOx/HRP and mPEG-HRP/GOx had uniform reaction rates, indicating that no imbalance had been introduced in the enzymatic activity due to conjugation (Figure S11, Supporting Information). The molecular substrate, glucose, could freely go through the protein membrane and undergo oxidation (GOx), generating hydrogen peroxide that subsequently was used to fuel the peroxidation of amplex red (HRP), which was also able to permeate the membrane (Figure 4b and 4c). The evolution of fluorescence in either functional protocell was entirely dependent upon the presence of both enzymes, with control experiments showing no background signal (Figure 4d i). Monitoring the reaction kinetics from the two protocell systems (with carefully monitored enzyme concentrations to maintain consistency), it was apparent that the product turnover was significantly increased (*ca.*10-fold) compared to free enzyme in solution owing to the increased local substrate concentration and reduced diffusional barrier between the two enzymes (Figure S12, Supporting Information). Comparing the two systems with each other, the GOx-membrane/HRP-cytosol system had a greater turnover, which was likely due to step-wise substrate processing of glucose → hydrogen peroxide being

reflected by the protocell structure so that glucose did not have to diffuse through the membrane before it could activate the first enzyme (in this case GOx) that was already displayed at the external interface – an active benefit of spatial organization (Figure S13, Supporting Information). Thereafter, we compared the GOx/HRP cascade when either enzyme was separately sequestered in distinct protocellular populations or when both enzymes were co-sequestered in a single population (Figure 4d). As expected, due to the reduced diffusional barrier when enzymes were co-sequestered, the reaction turnover was 1.33-fold higher as compared to the communicating GOx/HRP sub-populations (Figure 4d). With the ability to engineer functional membranes and activate enzyme cascades through spatial organization of active components this system is highly versatile and provides a platform for the development of hybrid protocells.

In order to further utilize the semi-permeable nature of protein membranes, and show the importance of spatial organization in the activation of enzymatic processes, we generated hybrid protocells based upon poly (diallyldimethylammonium chloride) (PDDA) and adenosine triphosphate (ATP).[7] To this end, we synthesized mPEG-amylase (following the same method as with BSA, GOx and HRP), confirming that the activity was retained by monitoring the oxidation of ABTS with amylose provided as a substrate (Figure S14, Supporting Information). Successful membranization of PDDA/ATP coacervates, loaded with fluorescent calcein, by mPEG-amylase (rhodamine labelled for visualization) clearly demonstrate the versatility of this approach, extending out to different enzymes and different types of coacervate (**Figure 5**a). By comparing the performance of two distinct configurations we could demonstrate the importance of spatial organization in the activation of enzymatic processes. When a hybrid protocell with an mPEG-amylase membrane (loaded with GOx and HRP in the coacervate cytosol) was exposed to a 70 kDa dextran solution, it

was able to fuel the cascade and generate fluorescent resorufin with a 4.3-fold increase in the internal fluorescence after 16 mins (Figure 5b and 5d). In contrast, hybrid protocells with an mPEG-GOx membrane (loaded with HRP and amylase in the coacervate cytosol) was unable to process the dextran substrate (Figure 5c). This difference arose due to the impermeable nature of the protein membrane towards higher molecular weight macromolecules like 70 kDa dextran, which could only be processed by the amylase-based membrane in order to feed glucose into the coacervate-based enzymes. In this way, we demonstrate the importance of spatial organization in transferring chemical information from the external to internal protocell environments and the ability of enzymatic membranes to successfully realize this process.

3. Conclusion

We have demonstrated a new type of hybrid protocell based on the spontaneous self-assembly of protein-polymer conjugates at the surface of coacervate microdroplets. The resulting protocells comprise a coacervate cytosol and proteinaceous membrane that can facilitate the investigation of biomolecular process such as chemical communication. This model integrates membrane-protected (and size-selective) compartmentalization with chemical enrichment via coacervate sequestration, which provides a versatile route to explore prebiotic molecular organization. Our studies indicate that protein membranes effectively stabilize coacervates microdroplets against uncontrolled coalescence, a key property in the transition from membrane-free to membranous protocells. Moreover, by substituting a model protein (BSA) for functional enzymes (in this case GOx HRP and amylase) as the basis of the membrane, it is possible to mimic chemical communication and explore pathways by which a single entity can respond to external stimuli through internal reaction processing. We expect such hybrid protocells will be an important tool that can be implemented in research to study the origins of cellular compartmentalization and the physicochemical properties of such a phenomenon.

4. Experimental Section

Synthesis of quaternized amylose (Q-Am): Quaternized amylose (Q-Am) was prepared by dissolving 150 mg of amylose and 280 mg of NaOH in 14.25 mL of Milli-Q at 35 °C. After complete dissolution of the amylose, 1.1 mL of 3-chloro-2-hydroxypropyltrimethylammonium chloride solution (65 wt% in water) was added dropwise into the stirring reaction mixture, which was subsequently left to react overnight. The final mixture was neutralized with acetic acid and dialysed extensively against water using dialysis tube with 3.5 kDa.

Synthesis of succinyl amylose (Su-Am): Succinyl amylose (Su-Am) was prepared by dissolving 100 mg of amylose and 185 mg of succinic anhydride in 15 mL of DMSO at 60 °C. After complete dissolution of the amylose, 5 mg of DMAP was added and the reaction mixture was left to stir for 16 hours. After the reaction, the mixture was diluted with 30 mL water and dialysed extensively against water using dialysis tube with 3.5 kDa.

Synthesis of Cationized Bovine Serum Albumin (BSA-NH_2), Cationized Glucose Oxidase (GOx-NH_2) and Cationized Peroxidase from horseradish (HRP-NH_2): Cationized bovine serum albumin (BSA-NH_2) was synthesized by carbodiimide activated conjugation of 1, 6-diaminohexane to aspartic and glutamic acid residues on the external surface of the protein. For this, a solution of 1, 6-diaminohexane (1.5 g, 12.9 mmol) was adjusted to pH 6.5 using 5 M HCl and added dropwise to a stirred solution of the protein (200 mg, 2.98 μmol). The coupling reaction was initiated by adding N-ethyl-N'-(3-(dimethylamino) propyl) carbodiimide hydrochloride (EDAC, 100 mg) immediately and again 50 mg after 5 h. The pH value was maintained at 6.5 using dilute HCl, and the solution was stirred for a further 6 h. The solution was then centrifuged to remove any precipitate, and the supernatant was dialyzed (dialysis tubing 12-14 kDa MWCO) extensively against Milli-Q water. Cationized Glucose

Oxidase (GOx-NH_2) and Cationized Peroxidase from horseradish (HRP-NH_2) were synthesized with the same method as BSA-NH_2.

Synthesis of mPEG-BSA, mPEG-GOx and mPEG-HRP: mPEG-BSA was synthesized by BSA-NH_2 and mPEG-SPA. For this, a solution of BSA-NH_2 (10 mg, 0.15 μmol) was prepared with pH 8.0 buffer. mPEG-SPA (10 mg, 2 μmol) solution was added dropwise to the stirred above protein solution and was stirred for a further 12 h. The solution was then centrifuged to remove any precipitate, and the supernatant was dialyzed (dialysis tubing 12-14 kDa MWCO) extensively against Milli-Q water. mPEG-GOx and mPEG-HRP were synthesized with the same method as mPEG-BSA.

RITC-labeled mPEG-BSA was synthesized by adding 25 μL of RITC DMSO solution (1.0 mg mL^{-1}) dropwise into a stirred mPEG-BSA aqueous solution (20 mg in 5 mL of PBS buffer pH 8.5). The mixed solution was mixed for 12 h. After that, the solution was dialyzed (dialysis tubing 3.5 kDa MWCO) extensively against Milli-Q water. RITC-labeled mPEG-GOx and RITC-labeled mPEG-HRP were synthesized with the same method as RITC-labeled mPEG-BSA.

Preparation of coacervate droplets: Q-Am and Su-Am were dissolved separately in pH 7.0 PBS at a concentration 1 mg/mL and coacervation was induced by mixing the solutions of Q-Am and Su-Am in a ratio of 2:1. The specific procedure was as following. 200 μL of a solution of Q-Am was stirred at 250 rpm in a vial and added dropwise 100 μL of Su-Am solution. As a result, coacervation was immediately and readily observed with the solution turned to be turbid.

Preparation of mPEG-BSA protected coacervate droplets: For the formation of mPEG-BSA stabilized coacervates, some aliquot of mPEG-BSA solution was added into the stirred and growing coacervate solution. To make the distribution of mPEG-BSA visible, a small aliquot of RITC-mPEG-BSA was injected in company. mPEG-GOx, mPEG-HRP and mPEG-Amylase coating coacervate droplets were prepared with the same way as mPEG-BSA.

Supporting Information

Supporting Information is available from the Wiley Online Library or from the author.

Acknowledgements

X.H and X.L thank NSFC (21871069 and 51873050) and the China Postdoctoral Science Foundation (2015M571401, X.L) for financial support. D.S.W. thanks the Ser Cymru II programme for financial support; this project received funding from the European Union's Horizon 2020 research and innovation programme under the Marie Skłodowska-Curie grant agreement No. 663830.

Conflict of Interest

The authors declare no conflict of interest.

Received: ((will be filled in by the editorial staff))
Revised: ((will be filled in by the editorial staff))
Published online: ((will be filled in by the editorial staff))

References

[1] a) S. Serrano-Luginbühl, K. Ruiz-Mirazo, R. Ostaszewski, F. Gallou, P. Walde, *Nature Reviews Chemistry* **2018**, *2*, 306; b) M. Li, X. Huang, T. Y. Dora Tang, S. Mann, *Curr. Opin. Chem. Biol.* **2014**, *22*, 1; c) P. Stano, P. L. Luisi, *Curr. Opin. Biotechnol.* **2013**, *24*, 633; d) Sven. Vogel, P. Schwille, *Curr. Opin. Biotechnol.* **2012**, *23*, 758.

[2] a) C. D. Keating, *Acc. Chem. Res.* **2012**, *45*, 2114; b) B. A. Grzybowski, W. T. S. Huck, *Nat. Nanotech.* **2016**, *11*, 585; c) X. Liu, P. Zhou, Y. Huang, M. Li, X. Huang, S. Mann, *Angew. Chem. Int. Ed.* **2016**, *55*, 7095.

[3] T. Trantidou, M. Friddin, Y. Elani, N. J. Brooks, R. V. Law, J. M. Seddon, O. Ces, *ACS Nano* **2017**, *11*, 6549.

[4] a) B. C. Buddingh, J. C. M. van Hest, *Acc. Chem. Res.* **2017**, *50*, 769; b) X. Liu, P. Formanek, B. Voit, D. Appelhans, *Angew. Chem. Int. Ed.* **2017**, *56*, 16233; c) J. Gaitzsch, X. Huang, B. Voit, *Chem. Rev.* **2016**, *116*, 1053; d) E. Rideau, R. Dimova, P. Schwille, F. Wurm, K. Landfester, *Chem. Soc. Rev.* **2018**, *47*, 8572.

[5] M. Li, X. Huang, S. Mann, *Small* **2014**, *10*, 3291.

[6] X. Huang, M. Li, D. C. Green, D. S. Williams, A. J. Patil, S. Mann, *Nat. Commun.* **2013**, *4*, 2239.

[7] a) D. S. Williams, S. Koga, C. R. C. Hak, A. Majrekar, A. J. Patil, A. W. Perriman, S. Mann, *Soft Matter* **2012**, *8*, 6004; b) K. A. Black, D. Priftis, S. L. Perry, J. Yip, W. Y. Byun, M. Tirrell, *ACS Macro Lett.* **2014**, 3, 1088; c) Q. Wang, J. B. Schlenoff, *Adv. Mater.* **2015**, 27, 2077; d) L. Zhang, L. Cai, P. S. Lienemann, T. Rossow, I. Polenz, Q. Vallmajo-Martin, M. Ehrbar, H. Na, D. J. Mooney, D. A. Weitz, *Angew. Chem. Int. Ed.* **2016**, 55,13470.

[8] P. Wen, X. Liu, L. Wang, M. Li, Y. Huang, X. Huang, S. Mann, *Small* **2017**, *13*, 1700467.

[9] a) J. P. Douliez, N. Martin, T. Beneyton, J. C. Eloi, J. P. Chapel, L. Navailles, J. C. Baret, S. Mann, L. Beven, *Angew. Chem. Int. Ed.* **2018**, *57*, 7780; b) S. D. Hann, K. J. Stebe, D. Lee, *Langmuir* **2017**, 33, 10107.

[10] S. M. Nomura, K. Tsumoto, T. Hamada, K. Akiyoshi, Y. Nakatani, K. Yoshikawa, *Chembiochem* **2003**, *4*, 1172.

[11] S. Sun, M. Li, F. Dong, S. Wang, L. Tian, S. Mann, *Small* **2016**, *12*, 1920.

[12] R. J. R. W. Peters, M. Marguet, S. Marais, M. W. Fraaije, J. C. M. van Hest, S. Lecommandoux, *Angew. Chem. Int. Ed.* **2014**, *53*, 146.

[13] a) K. Kurihara, M. Tamura, K. Shohda, T. Toyota, K. Suzuki, T. Sugawara, *Nat. Chem.* **2011**, *3*, 775; b) M. D. Hardy, J. Yang, J. Selimkhanov, C. M. Cole, L. S. Tsimring, N. K. Devaraj, *P. Natl. Acad. Sci. USA* **2015**, *112*, 8187.

[14] M. A. Grover, C. Y. He, M.-C. Hsieh, S.-S. Yu, *Processes* **2015**, *3*, 309.

[15] S. Mann, *Angew. Chem. Int. Ed.* **2008**, *47*, 5306.

[16] A. Zimber, Q. D. Nguyen, C. Gespach, *Cell Signal* **2004**, *16*, 1085.

[17] C. P. Brangwynne, C. R. Eckmann, D. S. Courson, A. Rybarska, C. Hoege, J. Gharakhani, F. Jülicher, A. A. Hyman, *Science* **2009**, *324*, 1729.

[18] S. Jain, J. R. Wheeler, R. W. Walters, A. Agrawal, A. Barsic, R. Parker, *Cell* **2016**, *164*, 487.

[19] C. F. Lee, C. P. Brangwynne, J. Gharakhani, A. A. Hyman, F. Julicher, *Phys. Rev. Lett.* **2013**, *111*, 088101.

[20] a) S. Koga, D. S. Williams, A. W. Perriman, S. Mann, *Nat. Chem.* **2011**, *3*, 720; b) N. N. Deng, W. T. S. Huck, *Angew. Chem. Int. Ed.* **2017**, *56*, 9736; c) S. Deshpande, F. Brandenburg, A. Lau, M. G. F. Last, W. K. Spoelstra, L. Reese, S. Wunnava, M. Dogterom, C. Dekker, *Nat. Commun.* **2019**, *10*, 1800.

[21] a) H. Chang, H. Jing, Y. Yin, Q. Zhang, D. Liang, *Chem. Commun.* **2018**, *54*, 13849; b) Y. Yin, L. Niu, X. Zhu, M. Zhao, Z. Zhang, S. Mann, D. Liang, *Nat. Commun.* **2016**, *7*, 1.

[22] D. S. Williams, A. J. Patil, S. Mann, *Small* **2014**, *10*, 1830.

[23] B. J. McKenna, H. Birkedal, M. H. Bartl, T. J. Deming, G. D. Stucky, *Angew. Chem. Int. Ed.* **2004**, *116*, 5770.

[24] T. Y. Dora Tang, C. Rohaida Che Hak, A. J. Thompson, M. K. Kuimova, D. S. Williams, A. W. Perriman, S. Mann, *Nat. Chem.* **2014**, *6*, 527.

[25] a) D. C. Dewey, C. A. Strulson, D. N. Cacace, P. C. Bevilacqua, C. D. Keating, *Nat. Commun.* **2014**, *5*, 4670; b) J. P. Douliez, N. Martin, C. Gaillard, T. Beneyton, J. C. Baret, S. Mann, L. Beven, *Angew. Chem. Int. Ed.* **2017**, *56*, 13689.

[26] A. F. Mason, B. C. Buddingh, D. S. Williams, J. C. M. van Hest, *J. Am. Chem. Soc.* **2017**, *139*, 17309.

[27] a) X. Huang, M. Li, S. Mann, *Chem. Commun.* **2014**, *50*, 6278; b) X. Huang, A. J. Patil, M. Li, S. Mann, *J. Am. Chem. Soc.* **2014**, *136*, 9225.

[28] F. Fanalista, S. Deshpande, A. Lau, G. Pawlik, C. Dekker, *Adv. Biosys.* **2018**, *2*, 1800136.

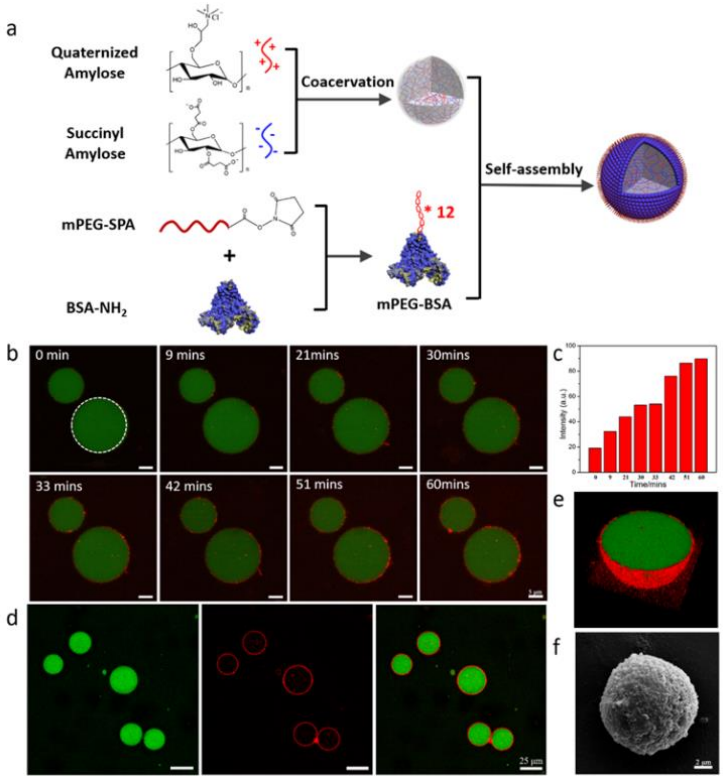

Figure 1. Formation of hybrid protocells through protein membranization of coacervate microdroplets. (a) General scheme for the preparation of membrane-stabilized hybrid protocell using cationic mPEG-protein conjugates on anionic coacervate microdroplets. (b) Spontaneous membranization of FITC-labelled coacervate (green) by fluorescent protein conjugates (red channel: RITC-mPEG-BSA) within an hour. (c) Fluorescence intensity increase of protein membrane marked by the while dashed circle in (b). (d) Stable hybrid protocells composed of fluorescein-loaded coacervates (green) and RITC-mPEG-BSA membrane (red) that do not undergo coalescence. (e) 3D confocal image and (f) scanning electron microscopy image of single hybrid protocell.

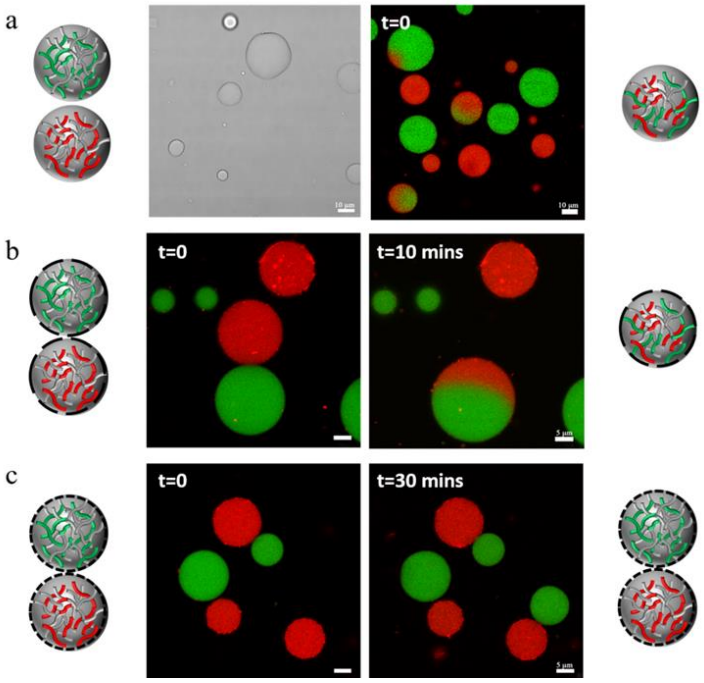

Figure 2. Stabilization of coacervate microdroplets by proteinaceous membrane. (a) Q-Am/Su-Am coacervates without stabilization coalesced rapidly. (b) After addition of 50 μL mPEG-BSA (50 mg/mL), coacervate microdroplets were partially stabilized with the appearance of coalescent phenomenon within 10mins. (c) After addition of 100 μL mPEG-BSA (50 mg/mL), complete stabilization of the coacervate microdroplets was achieved without any coalescent phenomenon observed during 30 mins *in situ* monitoring.

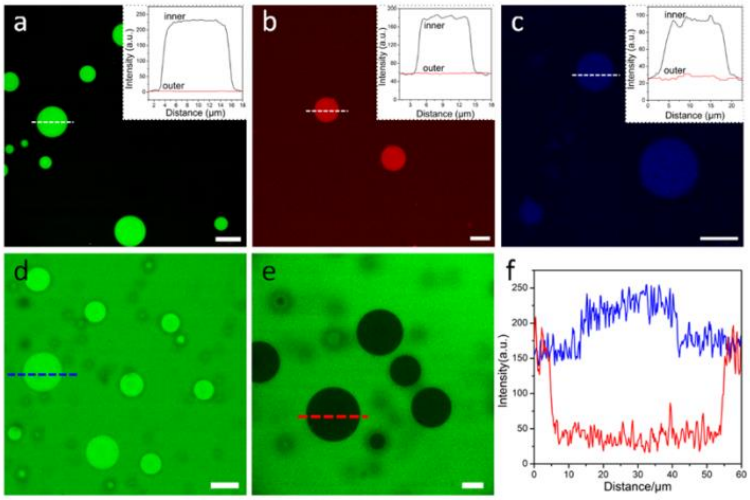

Figure 3. Dynamic sequestration and size-exclusion of hybrid protocells. Confocal fluorescence images to explore the sequestration behavior of (a) fluorescein, (b) rhodamine B, (c) NADH, (d) 4 kDa and (e) 10 kDa FITC-Dextran. The inner images in a-c were their corresponding fluorescence intensity line profiles. Based on these plottings, the partition coefficient K of the components in a-c were *ca.* 84.9, 3.1 and 3.6, respectively. (f) Fluorescence intensity line profiles of (d - blue) and (e - red), respectively. (Scale bars: a-c = 10 μm, d-e = 20 μm)

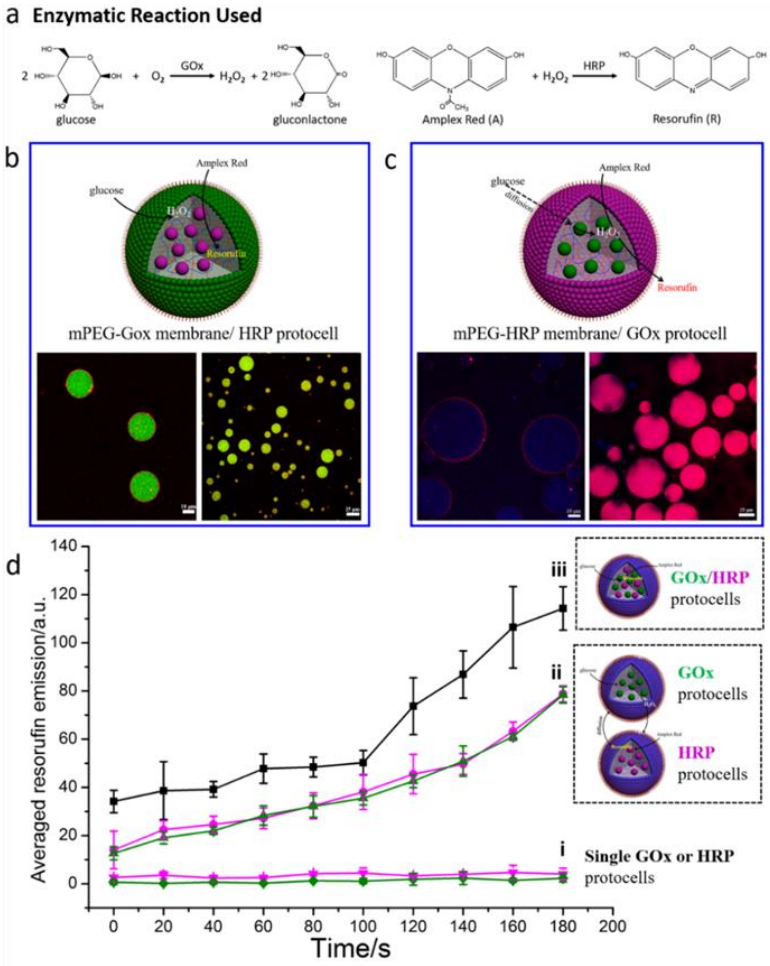

Figure 4. Spatial organization of enzyme cascade within hybrid protocells. (a) Enzymatic cascade reaction using GOx and HRP. (b, c) Schematic image and the corresponding confocal fluorescence images showed the spatial organization of the two enzymes within either the membrane or the coacervate cytosol. (b) HRP (fluorescein-labelled) sequestered in mPEG-GOx (rhodamine labelled) membranized protocells and (c) GOx (ATTO labelled) sequestered in mPEG-HRP (rhodamine-labelled) protocells. In both (b) and (c), glucose was added to initiate the cascade reaction that produced resorufin (red). (d) Analysis of the average resorufin fluorescence in the protocell experiments that i. GOx or HRP-loaded protocells (on their own), ii. mixed populations of protocells (green line: the enzymatic reaction rate in the GOx loaded protocell; pink line: the enzymatic reaction rate in the HRP loaded protocell) and iii. co-encapsulated protocells. Scale bars in (b) and (c): left 10 μm, right 25 μm.

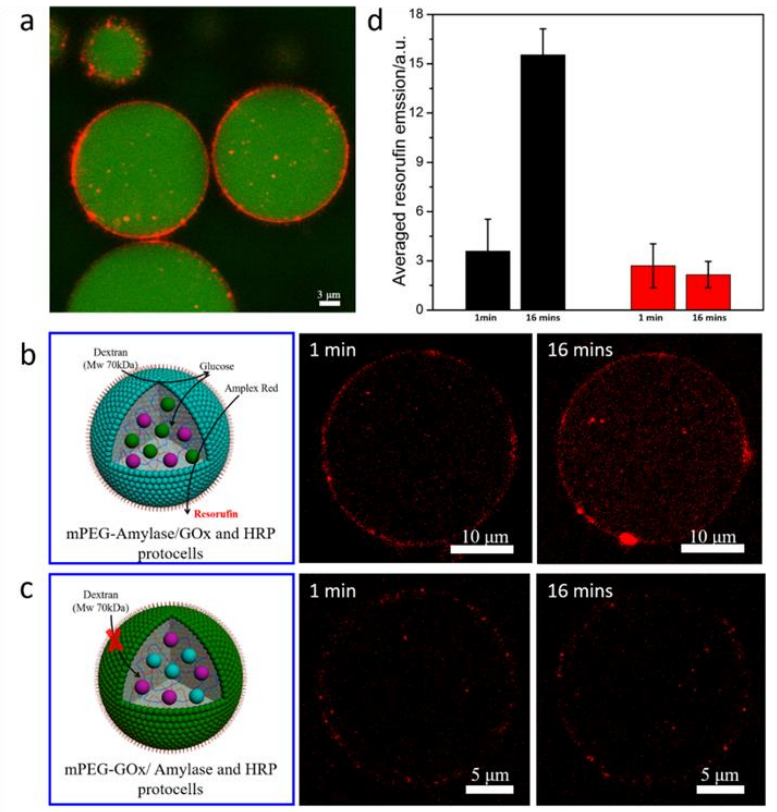

Figure 5. Size-regulation of enzymatic cascade (amylase-GOx-HRP) by spatial organization of specific enzymes in hybrid protocell. (a) PDDA/ATP coacervates loaded with calcein and coated with rhodamine-labelled mPEG-Amylase. Evolution of fluorescence signal (resorufin, red) in hybrid protocell with (b) mPEG-amylase membrane and (c) mPEG-GOx membrane (the other enzymes were sequestered inside the coacervate cytosol) over 16 mins. (d) The corresponding change of the fluorescence intensity of resorufin after 16 mins in b (black column) and c (red column).

Spatial Organization in Proteinaceous Membrane-Stablized Coacervate Protocells

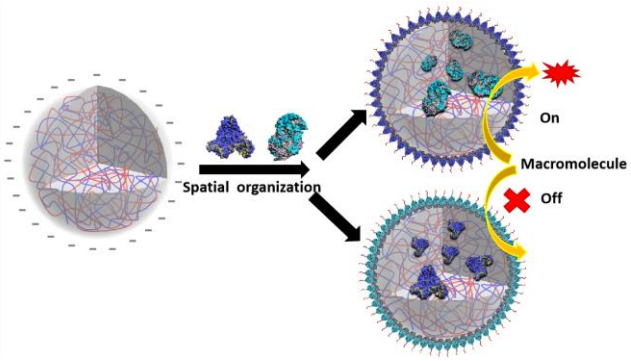

Supporting Information

Spatial Organization in Proteinaceous Membrane-Stablized Coacervate Protocells

Junbo Li, Xiaoman Liu, Loai K. E. A. Abdelmohsen,David S. Williams* and Xin Huang**

Materials

Amylose (M_W12000, Carbonsynth), Albumin from bovine serum (BSA, Sigma, 98%), Glucose Oxidase from spergillus niger (GOX, Sigma), Peroxidase from horseradish (HRP, Sigma), Glycine (Biosharp), 1,6-diaminohexane (Kermel), N-(3-dimethylaminopropyl)-N'-ethylcarbodiimide hydrochloride crystalline (EDAC, Sigma-Aldrich, 98%), Glucose (Sigma, ≥99.5%), NaOH (Sigma), $CuSO_4$ (Sigma), 3-chloro-2-hydroxypropyltrimethylammonium chloride (CHPTPA, TCI Europe, 65 wt% in water), Succinic anhydride (Aladdin, 99%), Dimethyl suifoxide (DMSO, Energy sulfoxide), 4-(dimethylamino) pyridine (DMAP, Sigma), mPEG-SPA (M_W 5000, Biomatrik), 2,4,6-trinitrobenzene sulfonic acid (TNBSA) solution (5 % (w/v) in H_2O, Sigma), FITC (Fluorescein isothiocyanate isomer I, Sigma 90 %), RITC(Rhodamine B isothiocyanate, Sigma), FITC-Dextran (fluorescein isothiocyanate-labeled dextran, M_W 4 kDa, 10 kDa, Sigma, 98 %), Dextran (M_W 70 kDa, Sigma), ABTS and Amplex Red were used as received without further purification. Milli-Q water was used to prepare all the solutions in this study.

Characterization methods

^{1}H NMR spectra were recorded using a BRUKER ADVANCED spectrometer operating at 400 MHz with D_2O as solvent at room temperature. Scanning electron microscope (SEM) were obtained on a SU8000 with the samples coated with 10 nm platinum. UV-vis spectra

were measured on a PerkinElmer spectrophotomer (Lambda 750S, USA). Zeta-potential and DLS measurements were conducted using Malvern Zetasizer Nano-ZSP. Optical microscopy image was performed on a Leica DMI8 manual inverted fluorescence microscope. Confocal images were obtained on a Leica SP5-II confocal laser scanning microscope attached to a Leica DMI 6000 inverted epifluorescence microscope. The analysis for the size of the protocells were conducted by the statistical result from *ca.* 80 particles in optical microscopy.

Determination of primary amine group on the surface of BSA-NH_2, GOX-NH_2 and HRP-NH_2 by TNBSA measurement

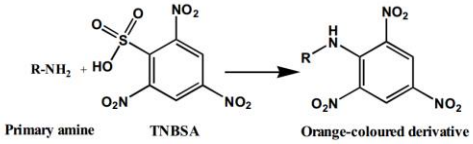

2,4,6-Trinitrobenzene sulfonic acid (TNBSA) is a rapid and sensitive assay reagent for the determination of free primary amine groups. Primary amines, upon reaction with TNBSA, form highly chromogenic derivatives, which can be measured at 345 nm by UV-vis spectroscopy. Typically, sample solutions of BSA-NH_2 (0.001-0.4 mg/mL) were prepared in 0.1 M sodium bicarbonate buffer (pH 8.5). The supplied 5 % TNBSA solution was diluted 250-fold in 0.1 M sodium bicarbonate buffer (pH 8.5). Then the diluted TNBSA solution (0.5 mL) was added to 1 mL of sample solution, and incubated at 37 °C for 2 hours. Next, 1 M HCl (0.2 mL) was added to each sample to stop the reaction. The UV-vis spectra of the solutions were recorded. To determine the concentration of amine, a standard primary amine absorbance curve was performed based on the same procedure using glycine as a standard compound. In comparison with glycine, the number of primary amine groups per BSA-NH_2 was determined to be *ca.* 80 on average.

The same method was used to measure the number of primary amine groups per GOx-NH_2 and HRP-NH_2. The number of primary amine groups per GOx-NH_2 and HRP-NH_2 was determined to be *ca.* 30 and 13 on average, respectively.

Determination of the number of mPEG on the surface of mPEG-BSA, mPEG-GOX and mPEG-HRP

Sample solutions of BSA were prepared with a series of concentration from 0 mg/mL to 2 mg/mL. A standard absorbance curve was performed according to the UV-vis spectra absorption at 277 nm. Record mPEG-BSA (1 mg/mL) absorbance value at 277 nm and put it into the standard curve to calculate the protein content. The number of mPEG per mPEG-BSA was determined to be *ca.* 12 on average.

The same method was used to measure the number of mPEG per mPEG-GOx and mPEG-HRP. The number of primary amine groups per mPEG-GOx and mPEG-HRP was determined to be *ca.* 11 and 6 on average, respectively. According above results, *ca.* 2.2 mg/mL mPEG-GOx amounts to 1 mg/mL GOx and *ca.* 1.7 mg/mL mPEG-HRP amounts to 1 mg/mL HRP.

Estimated degree of substitution (DS) of succinyl amylose by complexometric titration of Cu^{2+}

Prepare 12 parts of 0.5 mL of 3 mg/mL succinyl amylose solution with pH 7.0 and 4 mM copper sulfate solution, add 0.1~1.3 mL of copper sulfate solution to each Su-Am solution, and make the final volume up to 4mL. The absorbance at 244 nm was measured.

The carboxyl group and the hydroxyl group on Su-Am can interact with Cu ions. Su-Am is stoichiometrically coordinated with Cu ions to form complex and the concentration of the complex is proportional to the amount of copper sulfate. The charge density on the Su-Am molecular chain decreases and the chain tends to curl accompanying with the complex formed. Then, the hydroxyl group on the surface of Su-Am adsorbs on Cu ions. And the absorbance of the solution becomes steady with addition of copper sulfate.

The volume V of the copper sulfate corresponding to the maximum intersection point of the absorbance value is brought into the following formula to calculate the amount B (mmol/g) of carboxylate per gram of the sample.

$$B = \frac{2c_{(CuSO4)}V_{(CuSO4)}}{m} \quad (1)$$

The degree of substitution (DS) can be calculated as followed formula:

$$DS = \frac{162B}{1-100B} \quad (2)$$

m is the sample mass; 162 is the molar mass of the anhydroglucose unit of Su, and 100 is the molar mass of the net increase of each substituted hydroxy glucose unit. According to Figure S2, the DS of Su-Am was *ca.* 1.56.

Turbidimetry Measurement

Q-Am and Su-Am solutions were mixed at different stoichiometries to measure the coacervation behavior. Using a 2:1 stoichiometric ratio, the effect of salt concentration was evaluated by increasing [NaCl]. Turbidity was calculated as $100-\%T = 100-(100*10^{-Abs500})$.

Sequestration properties

The sequestration property of hybrid protocell was assessed by the difference at inner and outer of coacervate from confocal laser scanning microscope images. 0.5 μL of small molecules (fluorescein, rhodamine B and nicotinamide adenine dinucleotide) were added into 30 μL accomplished protocells. The fluorescence intensity of inner and outer of coacervates was significantly distinguishing. (All text parameters were the same).

The partition coefficient (*K*) was determined as $K=C_{coa}/C_s$, where C_{coa} and C_s were concentrations of the molecules in the coacervate and solution phases, respectively. The fluorescence intensity was proportional to the concentration of molecular. Hence, *K* can be roughly determined as $K=I_{coa}/I_s$.

Assay of Enzymatic catalytic reaction

Enzymatic cascade activity comparison of mPEG-GOx/HRP and mPEG-HRP/GOx was carried out by using Glucose and and ABTS (2,2'-azino-bis(3-ethylbenzothiazoline-6-sulfonic acid) diammonium salt) as substrates. The enzymatic reaction rate was monitored by UV-vis

spectroscopy at 414 nm using a 500 μL quartz cuvette containing 10 μL of enzyme aqueous mixture (1 mg/mL, mPEG-GOx/HRP or mPEG-HRP/GOx), 10 μL of ABTS aqueous solution (1 mg/mL) and 470 μL of PBS buffer (100 mM, pH 7.4). The reaction was initiated by addition of 10 μL of Glucose (1 mg/mL) and the enzymatic reaction was monitored for 15 mins.

The specific conditions for the data presented in the main paper are listed below:

Figure 1: 200 μL of 1mg/mL Q-Am was mixed with 100 μL of 1mg/mL Su-Am at 250 rpm, followed by the addition of 20 μL of 20 mg/mL (Figure 1a) and 50 mg/mL (Figure 1c) mPEG-BSA after 2 minutes of mixing. Particles were transferred to a confocal well and imaged.

Figure 2: 200 μL of 1 mg/mL Q-Am was mixed with 100 μL of 1 mg/mL RITC or FITC labeled Su-Am at 250 rpm, followed by addition of no mPEG-BSA (Figure 2a), 50 μL of 50 mg/mL (Figure 2b) and 100 mg/mL (Figure 2c) mPEG-BSA after 2 minutes of mixing. Particles were transferred to a confocal well and imaged for 10-30 minutes after a region located.

Figure 3: 200 μL of 1 mg/mL Q-Am was mixed with 100 μL of 1mg/mL Su-Am at 250 rpm. Particles were transferred to a confocal well after the formation of coacervates. Add fluorescein, rhodamine B, NADH, 4 kDa and 10 kDa FITC-Dextran to the coacervate droplets and image.

Figure 4: 200 μL of 1mg/mL Q-Am was mixed with 100 μL of 1 mg/mL Su-Am at 250 rpm, following the addition of 2.5 μL of 1 mg/mL FITC-HRP (Figure 4b) or ATTO-GOx (Figure 4c). After 2 minutes of mixing, 2.5 μL of 2.2 mg/mL mPEG-GOx/50 μL of 50 mg/mL mPEG-BSA (Figure 4b) and 2.5 μL of 1.7 mg/mL mPEG-HRP/50 μL of 50 mg/mL mPEG-BSA (Figure 4c) were added. Enzyme reaction was initiated by addition of 1 μL of 1 mg/mL Glucose and red fluorescence was observed by the addition of 1 μL of 0.1 mg/mL Amplex Red.

Figure 5: 100 μL of 40 mM PDDA was mixed with 100 μL of 20 mM ATP at 250 rpm, following the addition of 2.5 μL of 1 mg/mL HRP and 2.5 μL of 1 mg/mL GOx (Figure 5b), 2.5 μL of 1 mg/mL HRP and 2.5 μL of 1 mg/mL Amylase (Figure 5c). After 2 minutes of mixing, 2.5 μL of 1 mg/mL mPEG-Amylase/50 μL of 50 mg/mL mPEG-BSA (Figure 5b) and 2.5 μL of 2.2 mg/mL mPEG-GOx/50 μL of 50 mg/mL mPEG-BSA (Figure 5c) were added. Enzyme reaction was initiated by addition of 0.5 μL of 1 mg/mL Dextran (70 kDa).

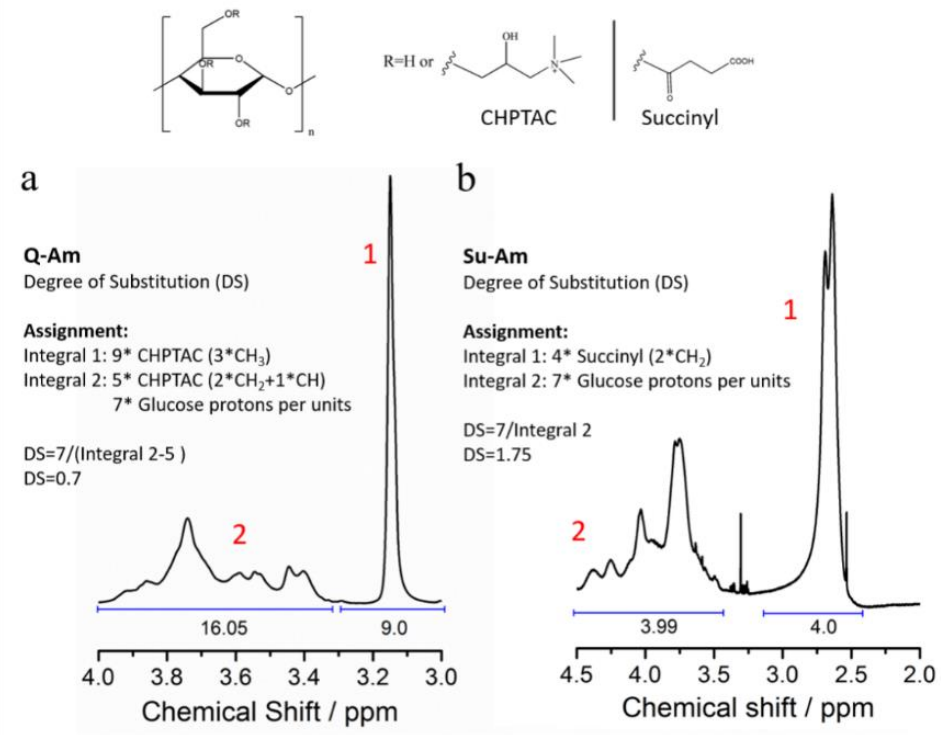

Figure S1. 1H NMR spectrum of charged amylose derivatives and the degree of substitution (DS) of quaternized (a) and succinyl (b) amylose.

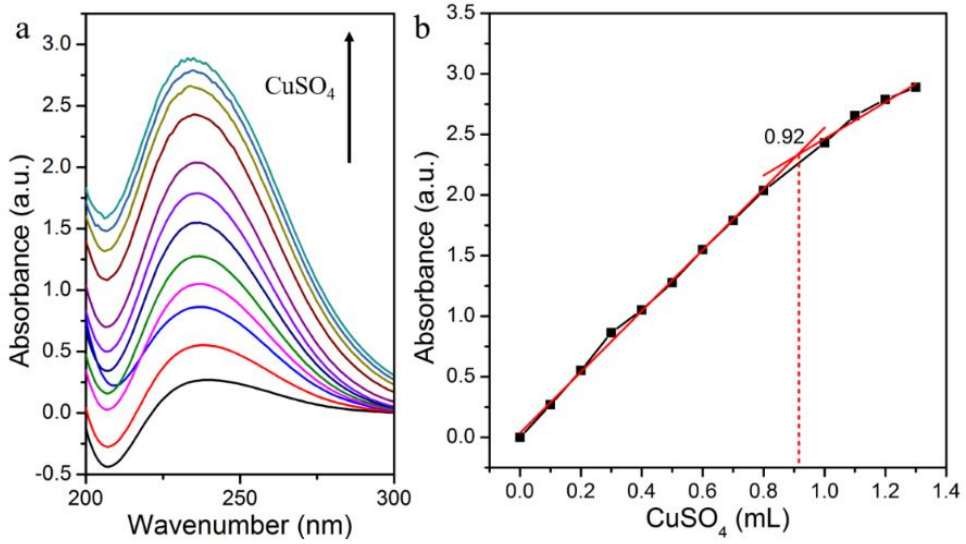

Figure S2. UV-Vis absorbance spectra of Su-Am-Cu(II) complex at 244 nm with the increasing of volume of $CuSO_4$ (a) and the corresponding curve for the absorbance values (b).

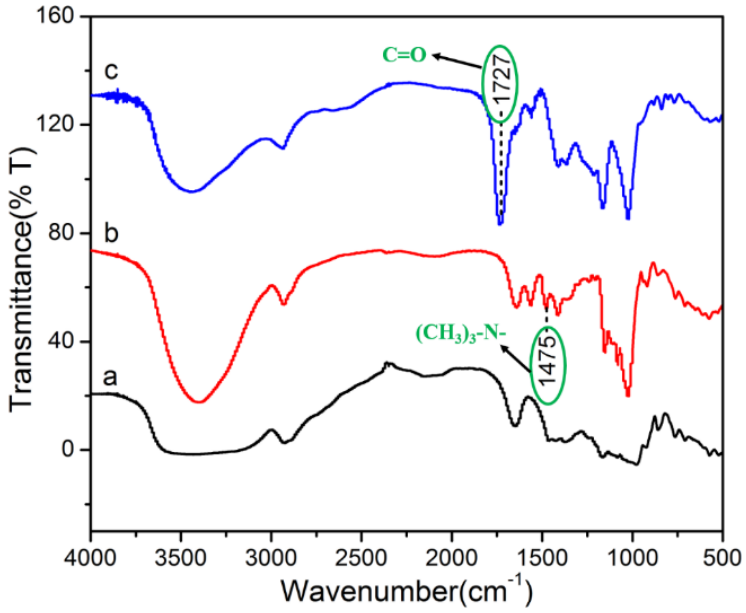

Figure S3. Infrared spectrogram of amylose (a), Q-Am (b) and Su-Am (c).

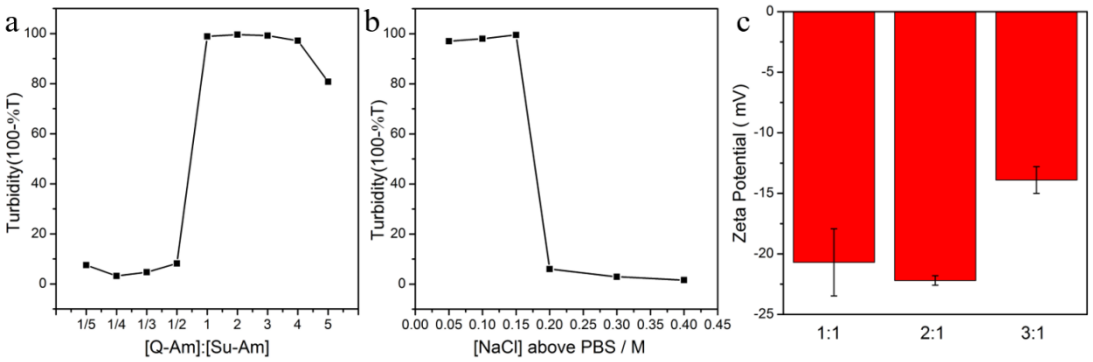

Figure S4. Turbidity measurements of Q-Am/Su-Am coacervates under (a) different stoichiometries and (b) different [NaCl] (above PBS). (c) Zeta-potential measurement of 1:1, 2:1 and 3:1 Q-Am/Su-Am coacervate droplets.

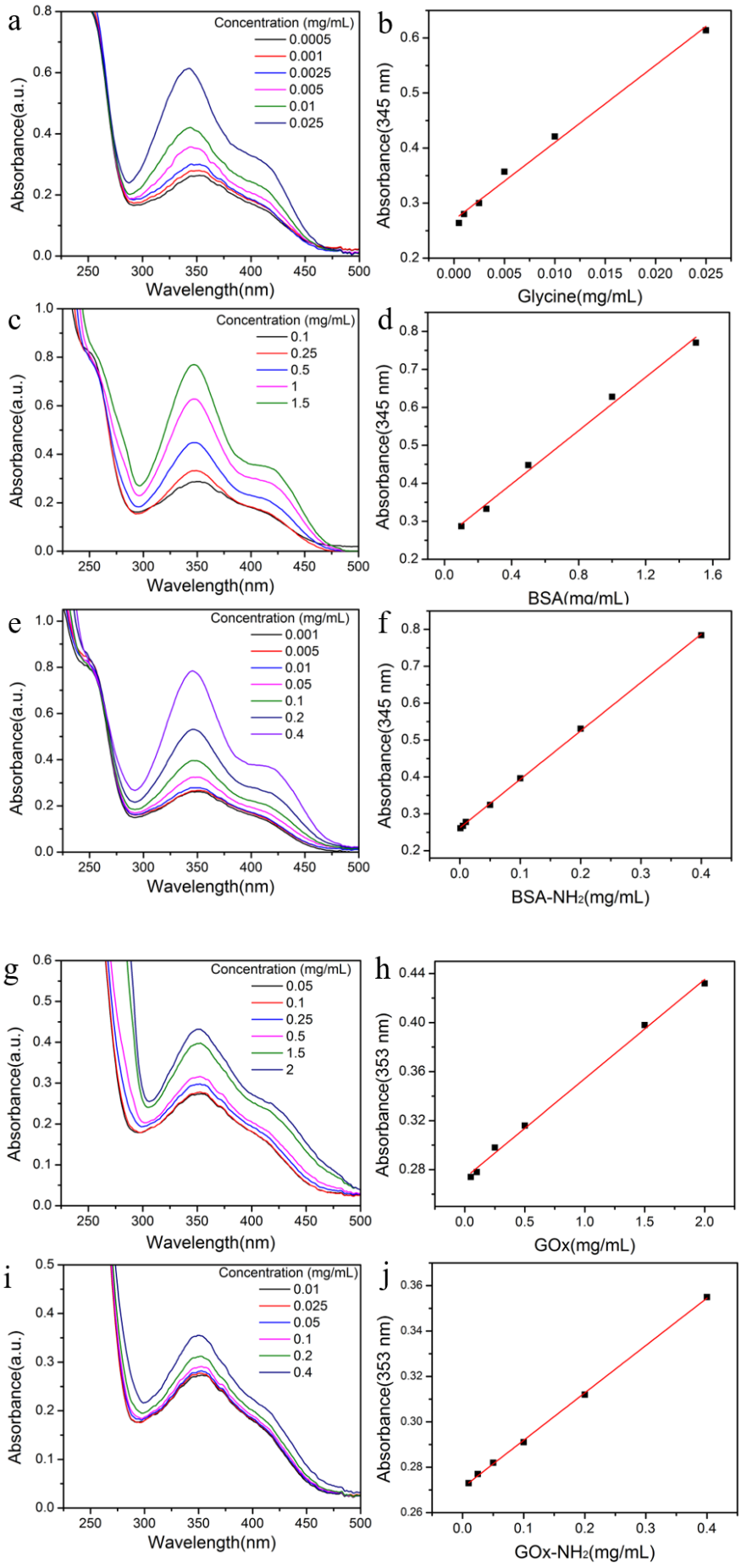
a
Concentration (mg/mL)
0.0005
0.001
0.0025
0.005
0.01
0.025
Absorbance(a.u.)
Wavelength(nm)
b
Absorbance(345 nm)
Glycine(mg/mL)
c
Concentration (mg/mL)
0.1
0.25
0.5
1
1.5
Absorbance(a.u.)
Wavelength(nm)
d
Absorbance(345 nm)
BSA(mg/mL)
e
Concentration (mg/mL)
0.001
0.005
0.01
0.05
0.1
0.2
0.4
Absorbance(a.u.)
Wavelength(nm)
f
Absorbance(345 nm)
BSA-NH2(mg/mL)
g
Concentration (mg/mL)
0.05
0.1
0.25
0.5
1.5
2
Absorbance(a.u.)
Wavelength(nm)
h
Absorbance(353 nm)
GOx(mg/mL)
i
Concentration (mg/mL)
0.01
0.025
0.05
0.1
0.2
0.4
Absorbance(a.u.)
Wavelength(nm)
j
Absorbance(353 nm)
GOx-NH2(mg/mL)

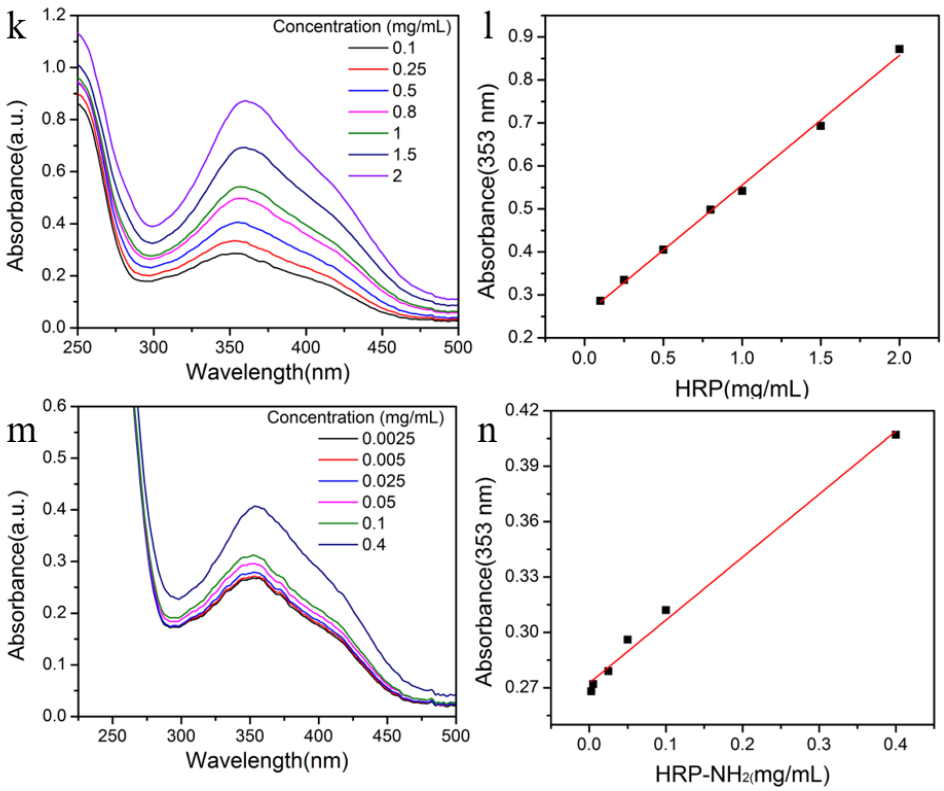

Figure S5. (a, c, e, g, i, k, m) UV-Vis spectra obtained for TNBSA/Glycine, BSA and BSA-NH_2, GOx and GOx-NH_2, HRP and HRP-NH_2 control assay, (b, d, f, h, j, l, n) corresponding calibration curve based on plotting the absorbance at 345 nm and 353 nm against the concentration of primary amine.

Table S1. Number of primary amine groups in BSA and BSA-NH_2

A (345 nm)	Glycine (mg/mL)	BSA (mg/mL)	Number (-NH_2)	BSA-NH_2 (mg/mL)	Number (-NH_2)
0.447	0.01262	0.53854	20.6	0.14077	78.8
0.626	0.02536	1.04786	21.3	0.27712	80.4
0.768	0.03447	1.45190	21.5	0.38529	80.9

Table S2. Number of primary amine groups in GOx and GOx-NH_2

A (353 nm)	Glycine (mg/mL)	GOx (mg/mL)	Number (-NH_2)	GOx-NH_2 (mg/mL)	Number (-NH_2)
0.316	0.00330	0.52752	12.5	0.21572	30.57
0.372	0.00729	1.21871	12.0	0.48651	29.94
0.432	0.01156	1.9593	11.8	0.77181	29.93

Table S3. Number of primary amine groups in HRP and HRP-NH_2

A (353 nm)	Glycine (mg/mL)	HRP (mg/mL)	Number (-NH_2)	HRP-NH_2 (mg/mL)	Number (-NH_2)
0.335	0.00465	0.27053	9.26	0.18312	13.5
0.495	0.01604	0.80033	10.7	0.65242	13.1
0.681	0.02928	1.41622	11.0	1.19799	13.2

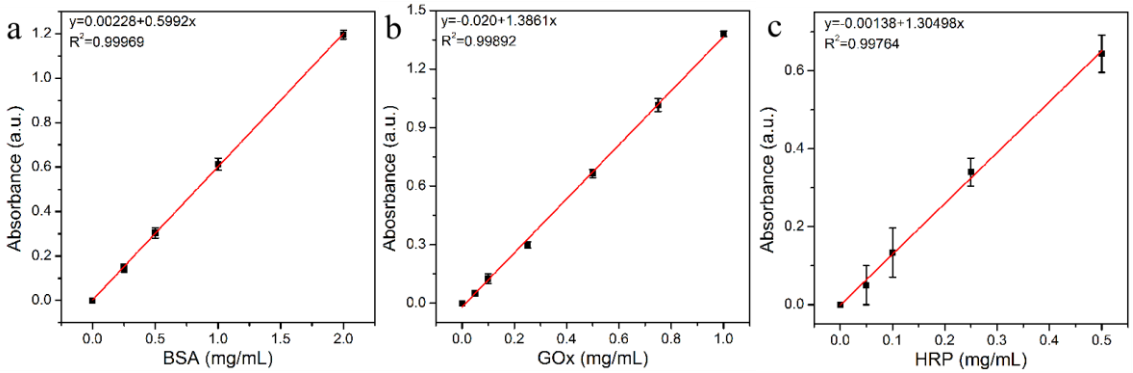

Figure S6. (a), (b) and (c) are UV-vis spectra of native BSA, GOx and HRP at different concentration in aqueous solution.

Table S4. Relative content of protein and mPEG in protein-mPEG conjugates

mPEG-BSA (mg/mL)	A_{277}	BSA (mg/mL)	mPEG (mg/mL)	n_{BSA}:n_{mPEG}
1.0	0.320	0.530	0.470	1:11.7
mPEG-GOx (mg/mL)	A_{277}	GOx (mg/mL)	mPEG (mg/mL)	n_{GOx}:n_{mPEG}
1.0	1.043	0.738	0.262	1:10.7
mPEG-HRP (mg/mL)	A_{402}	HRP(mg/mL)	mPEG (mg/mL)	n_{HRP}:n_{mPEG}
1.0	0.780	0.587	0.413	1:5.6

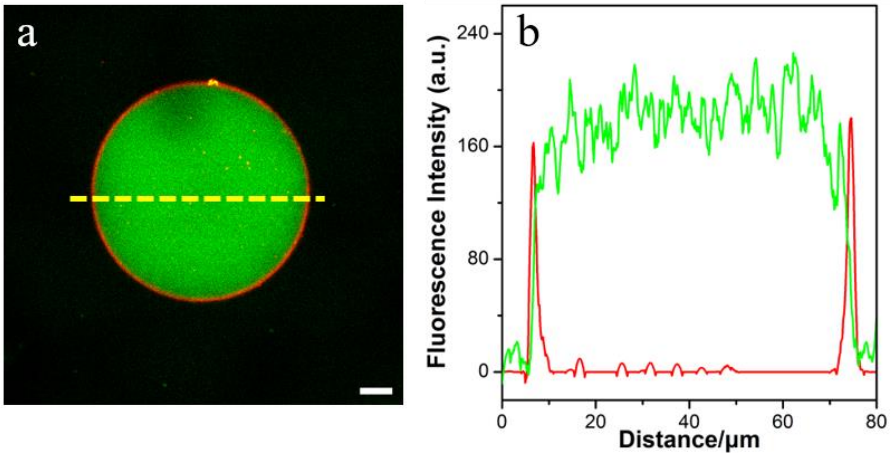

Figure S7. (a) Confocal micrographs of RITC-mPEG-BSA self-assembled on the surface of coacervate encapsulated with Fluorescein. Scale bars:10 μm. (b) Fluorescence intensity line profiles of selected coacervate are shown in the image (a).

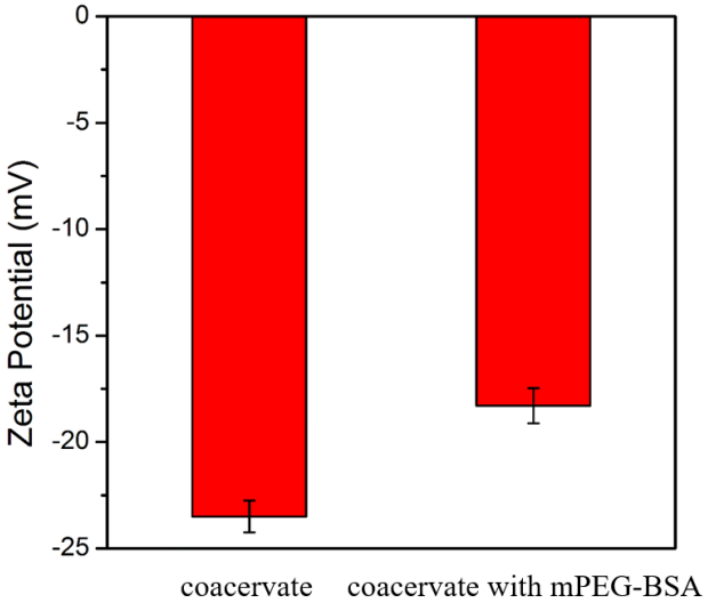

Figure S8. Zeta Potential characterization of coacervate and hybrid coacervate coated with BSA-mPEG.

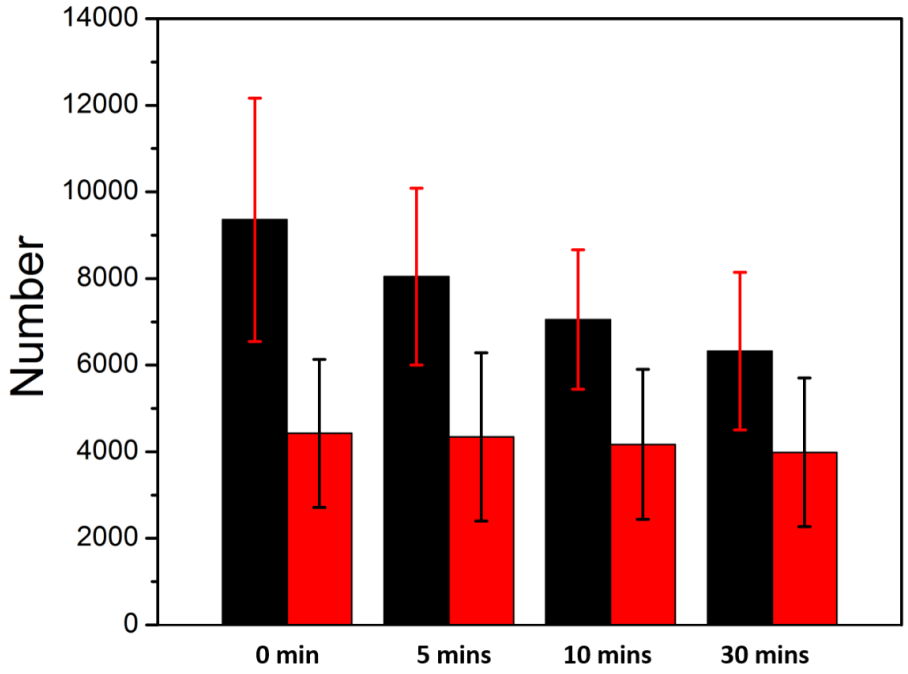

Figure S9. The statistics for droplet numbers for coacervate (black) and that with mPEG-BSA (red) within the same time.

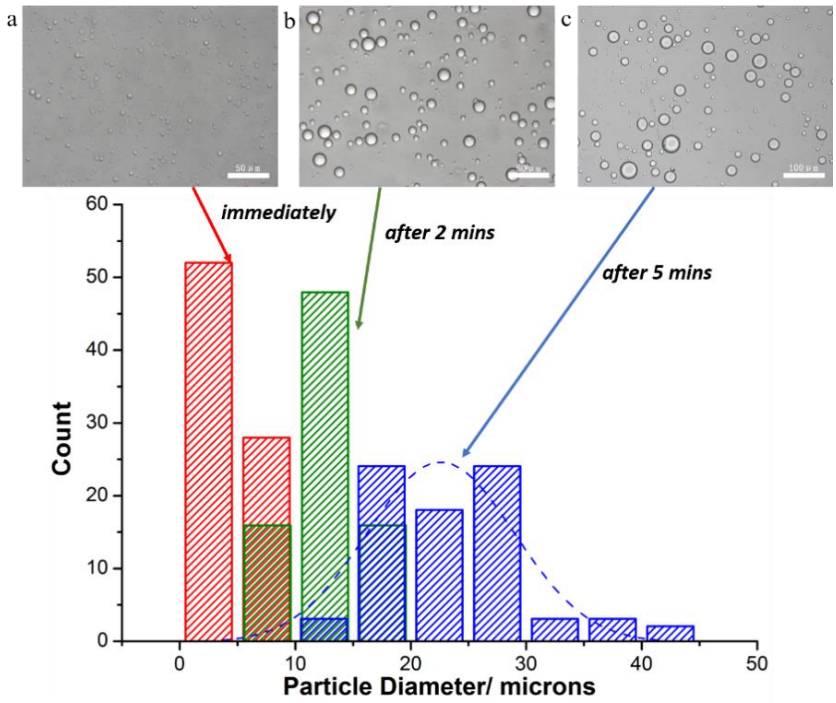

Figure S10. The size of coacervate can be controlled by adding the BSA-mPEG at different time points. BSA-mPEG is added when coacervation happened immediately (a), after 2 minutes (b) and 5 minutes (c). With the time prolonging, coacervate became larger. Each point counted *ca.* 80 particles for histogram statistics.

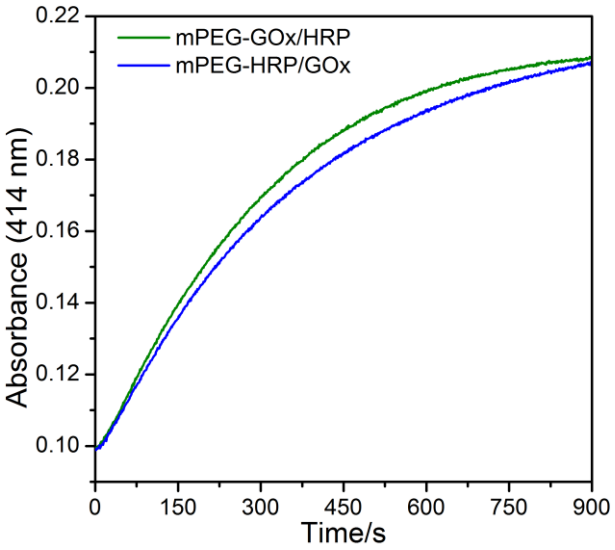

Figure S11. Enzymatic cascade activity comparison of mPEG-GOx with HRP (green) and mPEG-HRP with GOx (blue). The solution contains 5 μL of 2.2 mg/mL mPEG-GOx and 5μL of 1 mg/mL HRP for mPEG-GOx/HRP assay; 5 μL of 1.7 mg/mL mPEG-HRP and 5 μL of 1 mg/mL GOx for GOx/mPEG-HRP assay. The reaction was initiated by addition of 10 μL of 1 mg/mL glucose and 10 μL of 1 mg/mL ABTS.

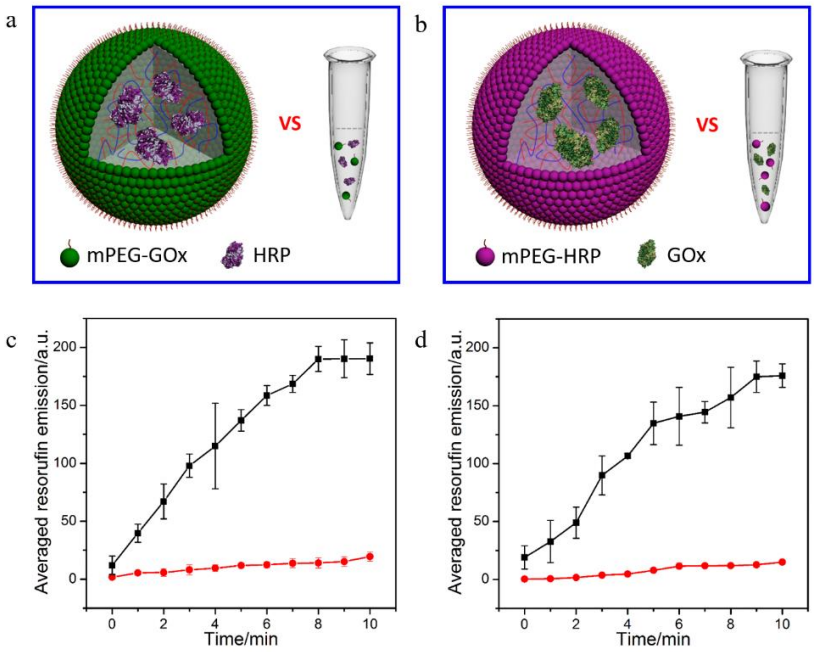

Figure S12. Enzymatic cascade rate comparison of mPEG-protein membraned coacervate with reaction in solution. (a) and (b) are the schemes of comparing coacervate encapsulated HRP with mPEG-GOx and the coacervate encapsulated GOx with mPEG-HRP with

corresponding mixing solutions. (c) and (d) are the analysis of the average resorufin fluorescence on the coacervates and solutions in above (a) and (b) (black curve: coacervate, red curve: solution).

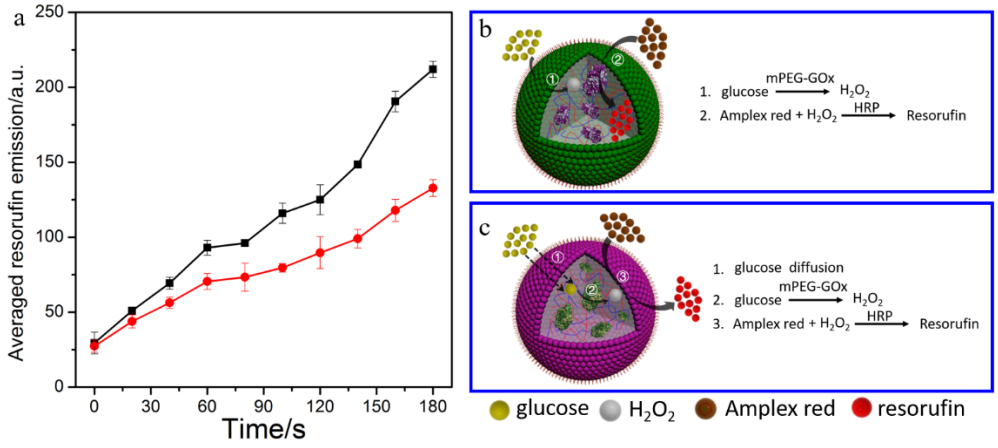

Figure S13. Analysis of the average resorufin fluorescence (a) and corresponding schemes of reactions in the hybrid protocell experiments that black curve in (a) corresponding to the mPEG-GOx membrane/HRP-loaded protocells in (b), and red curve in (a) corresponding to mPEG-HRP membrane /GOx-loaded protocells in (c).

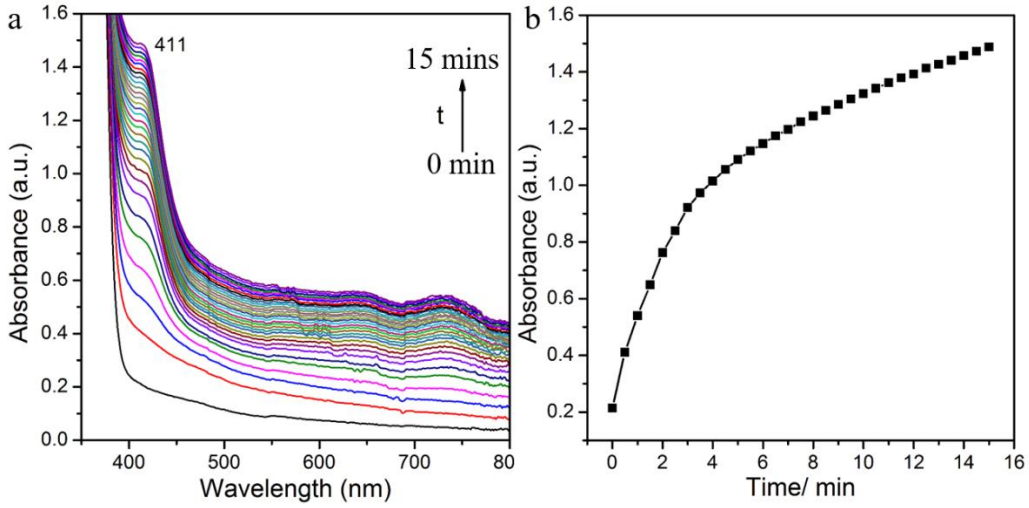

Figure S14. The activity of Amylase was remained due to the $ABTS^{+}$ production with the appearance of characteristic absorption at 411 nm after adding amylose into mPEG-Amylase, GOx and HRP mixing solution. (a) UV-Vis spectra and (b) corresponding absorbance at 411 nm with the time increasing.